ELSEVIER

Journal of Nuclear Materials 290–293 (2001) 25–32

journal of nuclear materials

www.elsevier.nl/locate/jnucmat

Mixed material formation and erosion

Ch. Linsmeier *, J. Luthin, P. Goldstraß

Max-Planck-Institut für Plasmaphysik, EURATOM-Association, Boltzmannstr. 2, D-85748 Garching, Germany

Abstract

The formation of mixed phases on materials relevant for first wall components of fusion devices is studied under well-defined conditions in ultra-high vacuum (UHV). This is necessary in order to determine fundamental parameters governing the basic processes of chemical reaction, material mixing and erosion. We examined the binary systems comprising of the wall materials beryllium, silicon, tungsten and titanium and carbon, the latter being both a wall material and a plasma impurity. Experiments were carried out to study the interaction of carbon in the form of a vapor-deposited component on clean, well-defined elemental surfaces. The chemical composition and the binding state are measured by X-ray photoelectron spectroscopy (XPS) after annealing treatments. For all materials, a limited carbide formation is found at room temperature. Annealing carbon films on elemental substrate leads to a complete carbidization of the carbon layer. The carbide layers on Be and Si are stable even at very high temperatures, whereas the carbides of Ti and W dissolve. The erosion of these two metals by sputtering is then identical to the pure metals, whereas for Be and Si a protective carbide layer can reduce the sputtering yields.

Keywords: Beryllium; Carbide; Carbon; Carbon deposition; Chemical erosion; Composite materials; Deposition; Diffusion; Erosion; First wall materials; High-Z material; Material mixing; Silicon; Titanium; Tungsten; XPS

1. Introduction

The design of modern fusion devices relies heavily on the selection of different materials for the plasma-facing wall parts which are exposed to different particle and heat loads. Besides the elements beryllium, tungsten and carbon, which are the favorite materials in the ITER design [1,2], silicon is currently used for wall conditioning [3,4]. Beryllium was very successfully used in JET as a first wall material and improved the impurity levels and plasma performance significantly [5–8]. Other designs involved titanium as limiter material [9]. Due to particle and heat loads, the wall material is eroded and migrates as plasma impurity to other parts of the vacuum vessel. In addition to the bulk wall materials recycling impurities like oxygen which are highly reactive are of concern. These impurities are deposited with particle energies ranging from thermal energy to several keV, depending on the ionization history and location of redeposition. Implantation and deposition of impurities lead to the formation of multi-elemental layers (e.g., [10]). The altered surfaces exhibit different qualities regarding the physical and chemical behavior compared to the originally designed first wall material. In particular, the physical and chemical erosion, thermal conductivity, hydrogen inventory properties are determined by stoichiometry, composition and chemical state of the surface of first wall materials.

Mixed phases have been addressed in the PSI literature. However, models proposed to describe the behavior of wall materials under plasma-exposed conditions in a fusion vessel are based solely on kinematic interactions, e.g., [11,12]. To predict the behavior of first wall materials for the strongly varying conditions within a real fusion experiment, the fundamental properties of the particle-surface interactions, surface chemistry and diffusion phenomena must be known. We therefore venture on projects which reduce interactions to few, well-controllable parameters to gain an insight into these processes.

* Corresponding author. Tel.: +49-89 3299 2285; fax: +49-89 3299 2279.

E-mail address: linsmeier@ipp.mpg.de (Ch. Linsmeier).

0022-3115/01/$ - see front matter
PII: S0022-3115(00)00428-1

2. Experimental

The task to determine the fundamental properties of the interaction of potential wall materials with impurities from the plasma requires very well-defined conditions. Parameters like surface composition and sample temperature must be controlled thoroughly. It is also necessary to have influence on the energy and composition of the interacting species. Therefore, all our experiments are carried out under ultra-high vacuum (UHV) conditions. Main tools for the characterization of mixed materials are photoelectron and ion spectroscopies. X-ray photoelectron spectroscopy (XPS) probes core-level transitions giving information on the specific element, including its chemical environment. Ion spectroscopies are accelerator techniques like the Rutherford backscattering spectroscopy (RBS). Our experimental setup ARTOSS [13] combines both surface sensitive tools and ion beam techniques available through a 3 MV tandem accelerator in one chamber. Also available in situ are the different ion sources for sample bombardment at energies between 100 eV and 20 keV, gas admission facilities and an electron beam evaporator, used to deposit carbon. For high-resolution XPS measurements, a second UHV system is available [14], equipped with a monochromatic Al X-ray source. This analysis chamber is connected to a preparation chamber where thin films can be prepared by electron beam evaporation from several sources. Gas admission is possible along with the formation of atomic species by means of a microwave discharge source [15]. The samples used in theses studies were polycrystalline foils of titanium and tungsten, a Si(1 0 0) wafer and a beryllium single crystal with (0 0 0 1) orientation. All samples are about 1 mm thick and have a surface area of approx. 1 cm^2. The surfaces are cleaned before carbon deposition by Ar^+ sputtering and/or heating. Carbon is deposited from an Omicron EFM3 evaporation source using high-purity (99.999%) carbon. The binding energies in the XPS spectra are referenced to the Au $4f_{7/2}$ signal at 84.0 eV determined on a clean gold surface.

3. Binary systems

3.1. Room temperature reactivity

Reactivity of the materials tungsten, titanium, silicon and beryllium at room temperature (~300 K) is studied at thermal carbon particle energies deposited from an electron beam evaporation source. XPS is used to determine the carbon amount on the W, Ti, and Si surfaces. In the Be experiments, the carbon layer thickness is additionally determined by RBS. To decide whether the deposited carbon is elementary or has reacted with the substrate material, the C 1s photoelectron peak is measured by XPS. Fig. 1 shows the C 1s spectra after depositing about two monolayers (ML) of carbon on Ti and Be and less than one ML on Si and W, respectively. The data are presented without background subtraction. In all four cases the C 1s intensity exhibits a peak at the binding energy characteristic for the respective carbide. The peak positions for the carbides are taken from the literature (Ti, Si, W [16]) or measured in a separate experiment (Be [18]). The hatched area in Fig. 1 indicates the binding energy range of elementary carbon. For the very thin carbon layers in the case of tungsten and silicon, almost all the C 1s intensity is in the carbide peak. For Si, a shoulder in the elementary carbon area is observed. The strong background in the W signal is due to a neighboring photoelectron peak (W $4d_{3/2}$) and not related to the C 1s signal. For greater coverages in the case of Ti and Be, the intensity in the elementary carbon area is larger. In the Ti spectrum, a distinct second peak is observed. The larger elementary signal in the case of

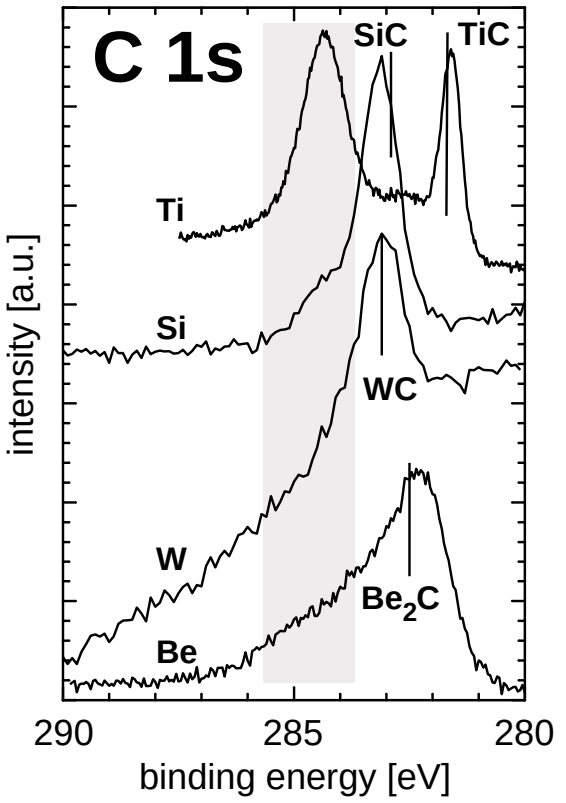

Fig. 1. XPS spectra in the C 1s energy range of thin carbon layers, deposited on the substrates at room temperature. The coverages for Si and W are below one monolayer, for Ti and Be about two monolayers. The vertical lines indicate the binding energies for the respective carbides, taken from the literature [16,18]. Peaks originating from elementary carbon appear in the shaded area.

Ti may be due to a larger carbon amount, since quantification is based in this case on the inelastic mean free path of the photoelectrons, whereas in the case of Be it is carried out by RBS measurement. Therefore, uncertainty in the Ti quantification is much larger than in the case of Be. Nevertheless, both elements exhibit a strong carbidic peak besides the intensity at higher binding energies.

The carbide formation starts at very low coverages and continues as long as there is a direct contact between carbon and the supporting element. Fig. 2 shows the development of the C 1s contributions of carbidic and elementary carbon (the latter separated into graphitic and disordered carbon) for the beryllium substrate. The carbon amounts are deposited sequentially on the clean Be substrate. RBS measurements are used to quantify the carbon coverage. The carbon modifications are distinguished by fitting three Gauss–Lorentz functions to the C 1s signal, each centered at the known peak positions [17,18]. As can be seen in Fig. 2, for low carbon coverage the reaction to Be_2C dominates over the elementary carbon deposition. This is true up to a carbon coverage of 9×10^{15} cm^{-2} where the intensities of carbidic and elementary carbon balance. From this coverage on the carbide amount saturates and further deposited carbon is accumulated in elementary form. The total carbon intensity increases linearly with coverage up to $\sim 2 \times 10^{16}$ cm^{-2}. For larger carbon surface densities, attenuation of the C 1s photoelectrons in the carbon layer on beryllium leads to a change in the slope of the curves. Since the carbide signal intensity starts to decrease, it can be concluded that the carbide is located at the carbon–substrate interface only and further carbon deposition leads to an increase in the elementary carbon coverage, but not to a further carbide formation.

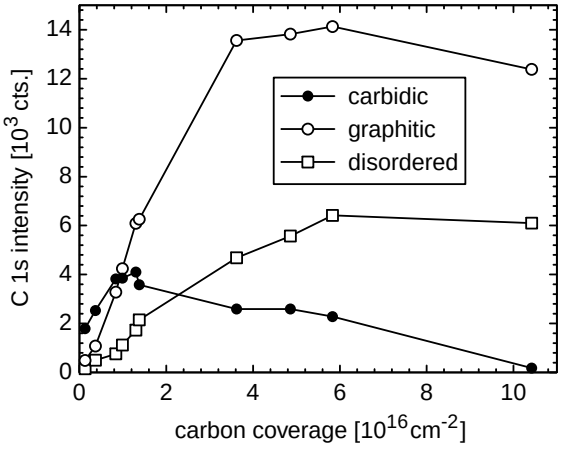

Fig. 2. Different states of carbon in deposited layers on beryllium, measured by XPS at room temperature. Plotted are the integrals of the components in the C 1s signal, determined by curve fitting, as a function of the carbon amount. The carbon coverage is determined by RBS.

3.2. Carbidization

The carbidization process of the elements W, Ti, Si and Be is studied by heating a carbon layer deposited on the samples at room temperature (thickness: several monolayers) to elevated temperatures and measuring the XPS spectra after each step. The corresponding spectra and the temperature profiles are shown in Fig. 3–8.

We begin the discussion of the carbidization process with beryllium. Fig. 3 shows the Be 1s and C 1s binding energy ranges of a carbon film on Be after evaporation (300 K) and after subsequent annealing steps. The Be 1s intensity is strongly attenuated by the overlying carbon film. From the Be 1s and C 1s intensities, a carbon layer thickness of 1.1 nm is calculated (assuming a carbon density of 1.8 g cm^{-3}). The C 1s peak indicates that the majority of the carbon is elementary, the shoulder at higher binding energies is due to a disordered graphite contribution [17]. A small contribution at 282.6 eV originates from the carbide at the carbon/metal interface. This thin carbidic layer is also seen in the Be 1s spectra. At the high energy side of the attenuated metallic Be peak a shoulder appears. Up to an annealing temperature of 473 K only small changes in the

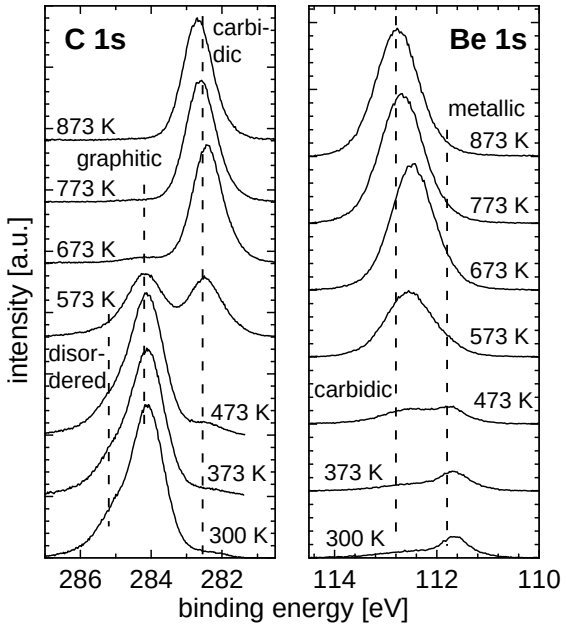

Fig. 3. Series of XPS spectra after deposition and annealing of a carbon layer on a Be (0 0 0 1) substrate. The annealing temperatures are indicated at the respective spectra. The broken lines indicate peak positions for metallic, carbidic and disordered species, respectively.

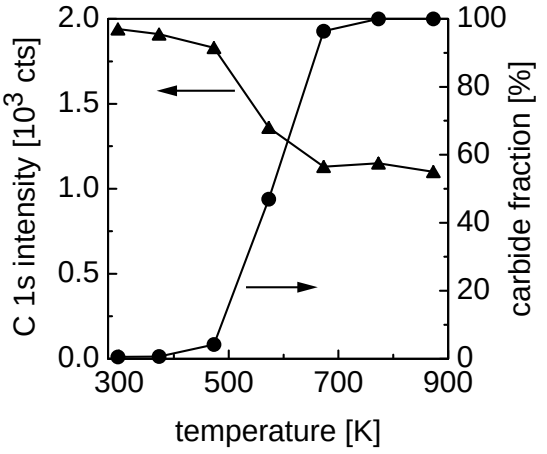

Fig. 4. Carbon intensity and carbide fraction in the total C 1s intensity, measured by XPS at a thin carbon film on Be (0 0 0 1).

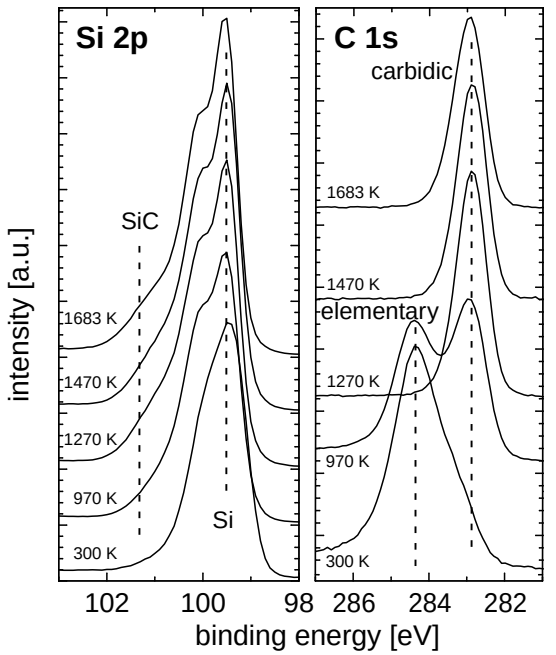

Fig. 5. Series of XPS spectra after deposition and annealing of a carbon layer on a Si (1 0 0) substrate. The annealing temperatures are indicated at the respective spectra. The broken lines indicate peak positions for elementary and carbidic species, respectively.

intensities are observed. In the C 1s region the disordered fraction of graphite decreases slightly and a small peak develops at the carbide position. These changes are also observed in the Be 1s spectra. Fig. 4 shows that up to 473 K the C 1s intensity and the carbide fraction of the C 1s signal change only to a small extent. A strong interaction between carbon and beryllium sets in above

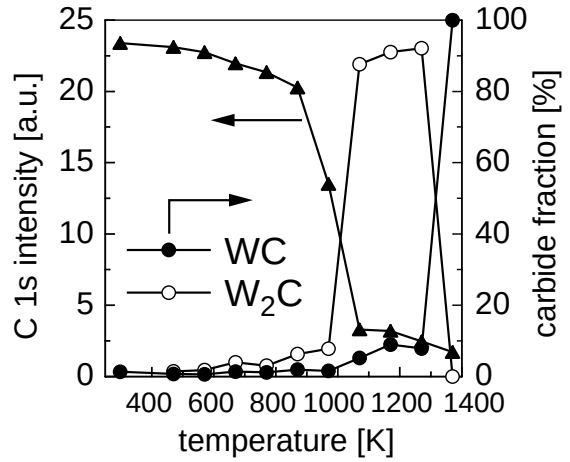

Fig. 6. Temperature profile measured by XPS from a thin carbon layer on polycrystalline tungsten. The circles indicate the carbide and subcarbide contributions to the total C 1s intensity, determined by peak fitting. The triangles show the decrease of the C 1s intensity with annealing temperature.

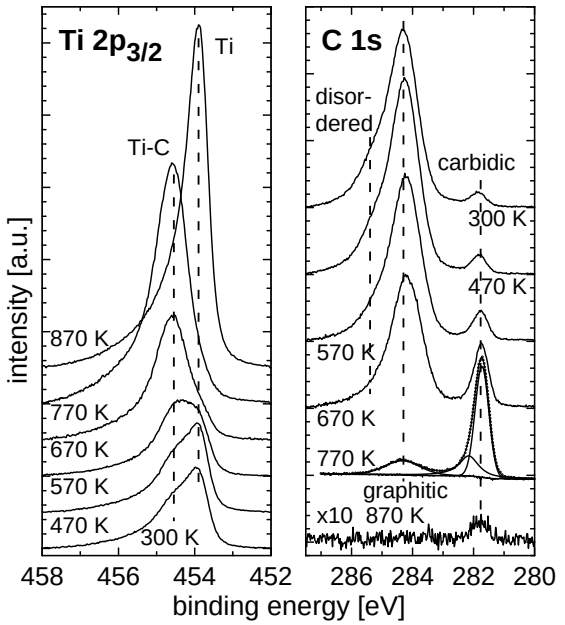

Fig. 7. Series of XPS spectra after deposition and annealing of a carbon layer on a polycrystalline Ti substrate. The annealing temperatures are indicated at the respective spectra. Please note that the Ti series runs bottom-up, whereas the C series starts with the top spectrum. The broken lines indicate peak positions for elementary and carbidic species, respectively. The 770 K spectrum shows the decomposition of the data by peak fitting in an elementary carbon peak and two carbidic peaks. The 870 K C 1s spectrum is enlarged by a factor of 10 compared to all other spectra.

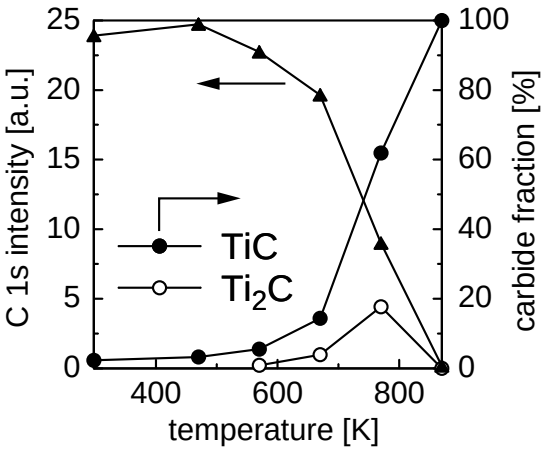

Fig. 8. Temperature profile measured by XPS from a thin carbon layer on polycrystalline titanium. The circles indicate the carbide and subcarbide contributions to the total C 1s intensity, determined by peak fitting. The triangles show the decrease of the C 1s intensity with annealing temperature.

473 K, the spectra after the 573 K step reveal more beryllium at the surface (intensity in the Be 1s region increases). The carbon binding energies indicate that both carbidic and elementary carbon are present in the surface layer, after 573 K approximately half of the carbon has reacted to carbide. The Be signal is already dominated by a peak at the binding energy of Be_2C at 112.8 eV with small intensity at the metallic Be position. The carbidization process proceeds as the annealing temperature is further increased and is almost complete already after annealing to 673 K. The carbide fraction in the C 1s signal reaches 100% and between 673 and 873 K no change in the carbon intensity is observed, as shown in Fig. 4. This demonstrates that carbon does not diffuse into the beryllium bulk upon further annealing once the carbidization is complete. At least up to this temperature the formed Be_2C layer on the beryllium substrate is stable. The interaction of a carbon layer with beryllium is discussed in greater depth in a separate contribution within this volume [19].

The carbidization of silicon is studied at a Si(1 0 0) surface with a carbon adlayer of approx. 0.3 nm thickness. Fig. 5 shows the XPS C 1s and Si 2p spectra for the annealing experiments up to 1683 K. Due to the small carbon coverage the Si 2p spectra are dominated by the elementary Si signal. It consists of a doublet which is not resolved in our spectra but leads to the asymmetric peak shape. Binding energies of the Si $2p_{3/2}$ peak for elementary (99.5 eV) and carbidic (101.3 eV) Si are indicated by broken lines. The C 1s spectrum taken directly after carbon evaporation exhibits a peak of elementary carbon and a small shoulder at the binding energy of SiC. This interfacial carbide is formed during carbon evaporation. Further reaction takes place at elevated temperatures. Almost half of the carbon (41%) has reacted after the 970 K annealing step which causes a more prominent asymmetry in the Si 2p peak and a second peak due to SiC in the C 1s region at 282.95 eV. All the carbon has reacted to SiC after annealing to 1470 K and no further changes are observable after 1683 K. SiC formed at the surface is stable up to this temperature. After 1270 K annealing step the C 1s intensity decreases only very little from 55.7% to 49.5% of its initial value.

The interaction of carbon with tungsten was described earlier [17] and partly also in a separate contribution in this volume [20] and therefore is only summarized here. Fig. 6 shows the carbidization behavior of polycrystalline tungsten between room temperature and 1370 K. Carbide is formed initially during the carbon evaporation at room temperature at the interface and the reaction proceeds with increasing substrate temperature. Between room temperature and 970 K the C 1s intensity decreases only slightly. In this temperature regime also only little additional subcarbide (W_2C) is formed. The C 1s intensity decrease therefore indicates an intermixing of carbon and tungsten in the surface layer to which XPS is sensitive. Above 970 K W_2C becomes the dominating phase. Above 1270 K the subcarbide is converted into tungsten carbide (WC). Unlike the carbide phases on beryllium and silicon, the tungsten carbides do not inhibit diffusion of carbon from the surface into the bulk. At the onset of W_2C formation where the carbon intensity is still 58% of its initial value the carbon concentration in the surface layer decreases to 14%. However, for higher temperatures the carbon amount does not change so rapidly any more. After the 1270 K treatment the intensity decreases only to 11%. The 1370 K annealing step then results in a further decrease to 7% of the room temperature intensity.

The carbidization of titanium proceeds very similar to the process on tungsten. Fig. 7 shows the XPS spectra in the Ti 2p and C 1s binding energy ranges taken after deposition of ca. 1 nm carbon on a polycrystalline titanium substrate and after the indicated annealing steps. The Ti peak consists of a metallic signal at 453.9 eV and a second signal from titanium carbide giving rise to the shoulder at 454.6 eV. The corresponding C 1s spectrum shows a large elementary carbon signal composed of graphitic and disordered contributions. The carbide peak is well separated at a binding energy of 281.8 eV. Upon annealing the carbon reacts with titanium under carbide formation. The processes of carbidization and carbon loss are depicted in Fig. 8. Up to a substrate temperature of 570 K the carbide intensity increases only slightly, the TiC fraction in the total C 1s intensity increases from initially 2.5% to 6.1%. The total carbon intensity does not change significantly. However, after this annealing temperature the data points can only be

fitted by introducing a further peak at a binding energy of 282.4 eV between the TiC and the elementary carbon. This is shown for the 770 K C 1s spectrum in Fig. 7. The peak integrals determined during the fit procedures are shown in Fig. 8. The total carbon intensity starts to drop above 570 K. This continues after the annealing steps at 670 and 770 K after which the carbon intensity remains only 38% of the initial value. The TiC peak intensity increases and becomes the dominating peak in the C 1s region after 770 K. Parallel to the TiC peak also the peak at 282.4 eV grows. In analogy to the tungsten system we attribute this peak to titanium subcarbides (Ti_8C_5, Ti_6C_5) [26,27] with a C 1s binding energy of around 282.4 eV. This is supported by observations in the literature where superlattice lines were found in neutron diffraction experiments of Ti–C alloys annealed between 1373 and 2273 K [21]. These results were recorded as tentative phases in the Ti–C phase diagram [22]. Unfortunately, the Ti 2p signals of metallic Ti and carbides are too close to shed light on the carbide phases. The intensity in this energy region is dominated by the carbide peak at a binding energy of 454.6 eV. The initially larger metallic contribution at 453.9 eV (82% of the peak area after carbon deposition) has decreased to a 16% fraction after annealing to 770 K. These values are estimates determined by fitting two asymmetric Doniach–Šunjić functions [23] to the Ti 2p peaks at the energies for titanium in metallic and carbidic chemical states. The next annealing step at 870 K leads to a complete dissolution of the carbide on the Ti surface. This is very different from the other elements under consideration so far. The Ti 2p region changes both in intensity and in the shape of the peak. The Ti $2p_{3/2}$ peak is fitted perfectly with only one Doniach–Šunjić function at a binding energy of 453.9 eV indicating that no carbide contributes to the signal. The intensity of this peak is the largest of the whole series of spectra. Correspondingly, the C 1s region shows hardly any peak. The signal depicted in Fig. 7 is enlarged by a factor of 10 compared to the other spectra and its integral is only 11 counts. The calculated carbon amount giving rise to this signal is 2% of a monolayer. It has to be noted, however, that the titanium surface becomes more and more reactive during the loss of carbon from the surface. During the last annealing steps at 770 and 870 K the surface accumulates oxygen which becomes the dominating signal after these temperatures. At present it is not clear whether this oxygen has any influence on the behavior described above.

3.3. Carbidization vs diffusion

From the last paragraph it becomes clear that two processes dominate the interaction of carbon with elemental surfaces: carbide formation and carbon diffusion. The chemical reaction between the carbon and the substrate starts in all cases already at room temperature and leads to a carbide layer at the interface between the deposited carbon and the substrate. However, in all cases studied so far the reactions come to a halt after one to several monolayers of carbide have been formed. The driving force of the carbidization reaction is the formation enthalpy of the carbides. All Gibbs energies (free enthalpies) for the materials under study here [24] are exergonic and therefore energy is released during the formation of carbides at room temperature. These negative enthalpies are the reason for the room temperature reactivity. The carbidization reaction can be written as the generic reaction equation:

$$\nu_M M + \nu_C C \rightleftharpoons \nu_{MC} MC + \Delta G_f \tag{1}$$

The law of mass action associated with this formation equation

$$[MC]^{\nu_{MC}} = [M]^{\nu_M}[C]^{\nu_C} e^{-(\Delta G_f/RT)} \tag{2}$$

illustrates that a more negative value of ΔG_f will increase the concentration of the carbide [MC]. Therefore, TiC is the most stable carbide in this selection, followed by Be_2C, SiC and the tungsten carbides (WC and W_2C). From Eq. (2) we can also see that the concentration of carbide depends on the concentration of both the element [M] and that of carbon [C], i.e., the availability of components for the reaction. At this point the diffusion of carbon into the respective substrate material becomes important. Fig. 9 summarizes the surface carbon concentration in the experiments described in Section 3.2. The curves are normalized to the initial carbon intensity after deposition at room temperature. In all cases the carbon layer thickness is thin enough that all carbon can be detected by XPS. The carbon intensity reflects the

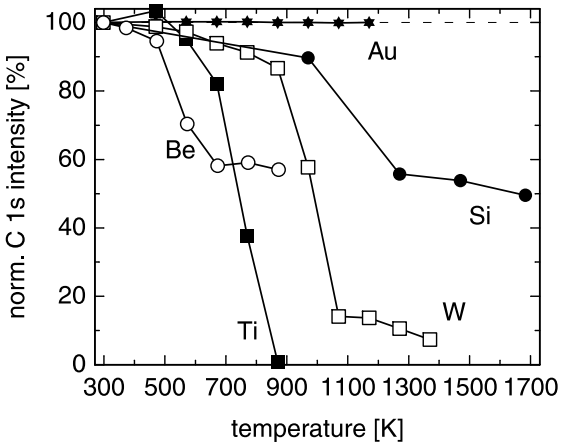

Fig. 9. Changes in the C 1s intensity measured by XPS during annealing of thin carbon films deposited on the indicated materials. The curves are normalized to the initial carbon intensity at room temperature (100%).

amount of carbon available in the surface layer. In addition to the elements Be, Si, Ti and W where carbide formation takes place, a reference experiment with a thin carbon layer on gold is plotted. Gold is inert and does not react with carbon under carbide formation. Moreover, carbon is insoluble in gold [22] and therefore no diffusive losses are expected. This is shown by the measured data points which stay constant at 100% level for all examined temperatures. It is observed that for all reactive elements the interaction can be divided into three phases. Phase I starts at room temperature and continues up to a temperature where the carbon intensity starts to drop. This phase is characterized by small carbon losses. We interpret this phase by an intermixing of the carbon layer with the substrate material which leads to substrate material in the analysis range of XPS. In Phase II the carbon intensity starts to decrease very fast. The start temperatures of this phase are also the temperatures where quantitative carbide formation sets in. Phase III finally is defined as the temperature range where the decrease of carbon intensity stops. This phase is only present in the cases of Be, Si and W. However, for W and, to a smaller extent for Si also, the carbon intensity decreases further even in phase III, but much slower than in phase II. For Ti no phase III is observed, the C intensity drops to zero at the end of phase II. In the cases of Be and Si the carbon intensity remains at a high level which indicates a stable carbide layer on top of the elemental substrate. The tungsten carbide, however, is not stable and dissolves into the substrate bulk. Other than in the case of titanium, there is a small amount of W_2C/WC remaining at the surface. The TiC is dissolved completely and at the final temperature only a trace of carbon can still be detected.

The different behavior of the carbon layers, the carbide formation and the dissolution of carbon in the substrate for the four elements Be, Si, W and Ti can be understood in terms of the structure of their respective carbides. Generally, solid carbides can be divided into three classes. Be_2C is an example of an ionic solid. The lattice constituents are ions and the interaction between them is electrostatic. Therefore, a diffusion of one lattice constituent involves the transport of charged particles in the field of the other ions. It can be qualitatively understood that transport of ions through the ionic lattice is difficult since the Coulomb barriers have to be overcome. The ionic compound Be_2C therefore remains stable even at much higher temperatures than the onset of the Be_2C formation. SiC represents the class of covalent solids. These solids are characterized by direct covalent bonds between the lattice constituents. In this picture it also becomes clear that diffusion of one component into a covalent solid needs directed bonds to be broken. Therefore, diffusion of carbon out of a SiC layer into the Si substrate is not favorable. From the covalent structure of SiC the stability of the carbide layer on the Si substrate can be understood. The situation for the transition metal carbides is different. Both Ti and W form metallic carbides where the carbon sits in the octahedral or trigonal prismatic sites in a metal atom spheres packing. Structure of the carbide is determined by the packing of metal atoms. In the case of the carbides WC and TiC carbon atoms occupy all octahedral sites. In W_2C and possibly also Ti subcarbides carbon fills half of the octahedral sites. Since there is no direct bond between metal and carbon atoms, a diffusion of carbon between different equivalent sites can explain the loss of carbon into the bulk substrate. In the case of tungsten a small concentration of WC remains stable even at high temperatures. In Ti, the diffusion of carbon is so high that the formed TiC layer is dissolved completely at elevated temperatures.

The final composition of the surface layer after an annealing treatment has profound influence on the erosion behavior of the material. With regard to sputtering, the amount of substrate material eroded by this process is proportional to the surface concentration of this constituent. If, as is the case for the elements Be and Si, a stoichiometric carbide layer is formed on the substrate and this layer remains stable at elevated temperatures, erosion by sputtering is only possible at the fraction of this element present in the carbide. In the case of Be_2C, the sputtering yield for Be is reduced by 1/3 compared to pure Be (without taking into account any surface binding energy effects). This reduction of the sputtering yield does not take place for materials like Ti and W where the formed surface carbide is not stable at elevated temperatures. After the carbide layer has been dissolved in these cases, the surface is dominated by the metal. Therefore, the sputtering yield of the pure metal is not reduced due to the dilution of the surface layer by carbon.

4. Summary and conclusions

All elements under study here (Be, Si, W, Ti) react with carbon already at room temperature. The thickness of the carbide layer is limited to the very interface between the carbon layer and the substrate, thus from one to several monolayers. Upon annealing to higher temperatures, the carbon layer reacts with the substrate material under carbide formation. The carbide layers on beryllium and silicon are stable up to very high temperatures, whereas on titanium and tungsten carbon diffusion into the bulk metal is important. This diffusion dissolves the carbide layer completely in the case of titanium and on tungsten only a small carbide amount is stable up to 1683 K. The different behavior of the elements can be understood in terms of the reaction enthalpy of carbide formation and of diffusion. The diffusion of the carbon in the host material is determined by the

structure of the respective carbide. Ionic (Be_2C) and covalent (SiC) carbides exhibit a strong bonding between the element and carbon and therefore no or only very small diffusion is observed. TiC and WC both are metallic carbides where the metal atom packing determines the structural properties. This is the reason why with both metal carbides a high diffusion of carbon is observed. The concentration of metal carbide present at a certain temperature therefore is determined by the reaction enthalpy (which is negative in all cases here and therefore favors carbidization over decomposition) and the availability of carbon for the carbide formation. If carbon is removed from the equilibrium, the carbide at the surface is decomposed. This has a large impact on the sputtering yield: the yield of the element under consideration in a mixed material is determined first of all by the stoichiometry at the surface. If the element fraction is reduced by compound formation, less of this element will be sputtered. If the carbide layer, however, is removed by carbon diffusion into the bulk, the surface concentration and also the sputtering yield of this element are similar to the pure elemental surface.

In extension to the binary systems discussed in this paper ternary mixtures between a wall material, carbon and oxygen as an impurity in fusion plasmas are of great importance. Several new phenomena regarding the surface reactivity and erosion properties are observed. Due to limited space, the ternary systems Be–C–O and W–C–O cannot be discussed here. We direct the reader to the respective contributions in these proceedings [20,25].

References

[1] ITER Project, Detailed Design Document, IdoMS# G 16 DDD 2 96-11-27 W.
[2] R.A. Anderl, R.A. Causey, J.W. Davis, R.P. Doerner, G. Federici, A.A. Haasz, G.R. Longhurst, W.R. Wampler, K.L. Wilson, J. Nucl. Mater. 273 (1999) 1.
[3] J. Winter, H.G. Esser, G.L. Jackson, L. Könen, A. Messiaen, J. Ongena, V. Philipps, A. Pospieszczyk, U. Samm, B. Schweer, B. Unterberg, the TEXTOR Team, Phys. Rev. Lett. 71 (1993) 1549.
[4] V. Rohde, R. Neu, R. Dux, T. Härtl, H. Maier, J. Luthin, H.G. Esser, V. Philipps, the ASDEX Upgrade Team, ECA vol. 23J (1999) 1513.
[5] J.T. Thomas, the JET team, J. Nucl. Mater. 176&177 (1990) 3.
[6] R. Satori, G. Saibene, D. Goodall, E. Usselmann, P. Coad, D. Holland, J. Nucl. Mater. 176&177 (1990) 624.
[7] P. Rebut, M. Hugon, S. Booth, J. Dean, K. Dietz, K. Sonnenberg, M. Watkins, JET-R(85)03, JET Joint Undertaking, Abington, 1985.
[8] E. Bertolini, Fus. Eng. Design 27 (1995) 27.
[9] P. Grigull et al., W7-AS Team, NBI Team, ECRH Group, J. Nucl. Mater. 196–198 (1992) 101.
[10] R. Behrisch, M. Mayer, C. García-Rosales, J. Nucl. Mater. 233–237 (1996) 637.
[11] D. Naujoks, R. Behrisch, In: Proceedings of the International Conference on Plasma Physics, Innsbruck, vol. 16C, part II, 1992, p. 843.
[12] Y. Hirooka, Fus. Eng. Design 37 (1997) 299.
[13] Ch. Linsmeier, P. Goldstraß, K.U. Klages, Phys. Scr. (submitted).
[14] S. Miller, G. Berning, H. Plank, J. Roth, J. Vac. Sci. Technol. A 15 (1997) 2029.
[15] Ch. Linsmeier, J. Wanner, Surf. Sci. 454–456 (2000) 305.
[16] J.F. Moulder, W.F. Stickle, P.E. Sobol, K.E. Bomben, in: J. Chastain (Ed.), Handbook of X-Ray Photoelectron Spectroscopy, Perkin–Elmer, Eden Prairie, MN, 1992.
[17] J. Luthin, Ch. Linsmeier, Surf. Sci. 454–456 (2000) 78.
[18] P. Goldstraß, Ch. Linsmeier, Nucl. Instrum. and Meth. B 161–163 (2000) 411.
[19] P. Goldstraß, K.U. Klages, Ch. Linsmeier, J. Nucl. Mater. this volume.
[20] J. Luthin, Ch. Linsmeier, these Proceedings.
[21] H. Goretzki, Phys. Status Solidi 20 (1967) K141.
[22] T.B. Massalski, H. Okamoto, P.R. Subramanian, L. Kacprzak, Binary Alloy Phase Diagrams, 2nd Ed., Version 1.0, ASM International, Materials Park, OH, 1996.
[23] S. Doniach, M. Šunjić, J. Phys. C: Solid St. Phys. 3 (1970) 285.
[24] I. Bahrin, Thermochemical Data of Pure Substances, 3rd Ed., Vol. 1&2, Weinheim, 1995.
[25] P. Goldstraß, Ch. Linsmeier, these Proceedings.
[26] N.V. Dzahalabadze, B.G. Eristavi, N.I. Maisuradze, E.R. Kuteliya, Phys. Metals Metall. 86 (1998) 59.
[27] B.V. Khaenko, S.Ya. Golub, M.P. Arbuzov, Kristallografiya 25 (1980) 112.